Phononic band gap in random spring networks

Kezhao Xiong,[1,2,*] Jie Ren,[3] Fabio Marchesoni,[3,4] and Jiping Huang[1,†]

[1]*Department of Physics, State Key Laboratory of Surface Physics, and Key Laboratory of Micro and Nano Photonic Structures (MOE), Fudan University, Shanghai 200438, China*

[2]*College of Sciences, Xi'an University of Science and Technology, Xi'an 710054, China*

[3]*MOE Key Laboratory of Advanced Micro-Structured Materials and Shanghai Key Laboratory of Special Artificial Microstructure Materials and Technology, School of Physics Science and Engineering, Tongji University, Shanghai 200092, China*

[4]*Department of Physics, University of Camerino, 62032 Camerino, Italy*

(Received 6 December 2022; revised 27 August 2023; accepted 7 September 2023; published 11 October 2023)

We investigate the relation between topological and vibrational properties of networked materials by analyzing, both numerically and analytically, the properties of a random spring network model. We establish a pseudodispersion relation, which allows us to predict the existence of distinct transitions from extended to localized vibrational modes in this class of materials. Consequently, we propose an alternative method to control phonon and elastic wave propagation in disordered networks. In particular, the phonon band gap of our spring network model can be enhanced by either increasing its average degree or decreasing its assortativity coefficient. Applications to phonon band engineering and vibrational energy harvesting are briefly discussed.

DOI: 10.1103/PhysRevE.108.044306

I. INTRODUCTION

As an interdisciplinary tool, network theory cuts through the boundaries of information, life, social, and material sciences. It spawned disruptive innovations and remarkable new scientific discoveries [1–9]. In the past three decades, much effort has gone into understanding phonon transport in networked media. These include amorphous networks [10,11], random spring networks [12], randomly bond-diluted triangular lattices [13], cross-linked polymer chains [14], and fiber composites [15], to name but a few. Unexpected wave propagation phenomena have been reported when using such materials in frequency filters, waveguides, emitters, shields, and topological insulators [16–23], with potential applications in numerous technological contexts, such as noninvasive diagnostics, medical imaging, and acoustic devices [24–26].

As of today, it is well recognized that elastic wave propagation in a network depends not only on the elastic moduli of its components, but also on its overall stiffness [27,28]. For instance, the acoustic characteristics of molecular chain networks change significantly by structural deformation [15,29]. However, earlier studies mainly focused on the relation between vibrational and mechanical properties of the networks, but seldom investigated the role of their topological properties. This is because disorder in network structures breaks translation invariance, a question that has long vexed physicists.

The topology of a network is characterized by a number of statistical parameters, such as average degree, assortativity coefficient, clustering coefficient, small-worldness, and closeness centrality [9,30–32]. Among such parameters, the average degree and the assortativity coefficient are best suited to characterize networked materials. For instance, the average degree quantifies the density of molecular chain networks, while the assortativity coefficient can be related with the node connectivity in cross-carbon nanotubes [33–35]. Nevertheless, little is known so far about how these two parameters impact the vibrational properties of networked materials and thus their wave propagation properties. In this paper, we propose a random spring network model with tunable topological parameters especially designed for this purpose. As a result, we develop an effective method to control the phonon band gap in disordered networks.

II. NETWORK MODEL

Our network model is constructed as follows. First, we generate a two-dimensional (2D) regular square lattice with $N = n \times n$ identical nodes of mass m. Each node can be uniquely identified by either a couple of row-column indices, (q, p), or by a single index $j = (q-1)n + p$. An example of a square lattice with $n = 10$ is displayed in Fig. 1(a). Secondly, we randomly pick a node from an odd-numbered column and an even-numbered row [denoted by a blue node in Figs. 1(b)–1(d)], and then randomly connect it to one of its four nearest neighbors at the catercorners. Upon repeating this process, M new diagonal links are added to the original regular lattice, thus creating a disordered network with average degree $\langle k \rangle = (1/N)\sum_j k_j = 4 + 2M/N$, where k_j is the number of links connected to node j (node degree). Repeated links are discarded in the process. Two realizations of this procedure obtained from the regular lattice of Fig. 1(a), respectively, for $M = 20$ and 55, are shown in Figs. 1(b) and 1(c). Note that for $M = N$, all blue nodes are connected with their catercorner neighbors, which results in the new regular topology of

*xiongkezhao@outlook.com
†jphuang@fudan.edu.cn

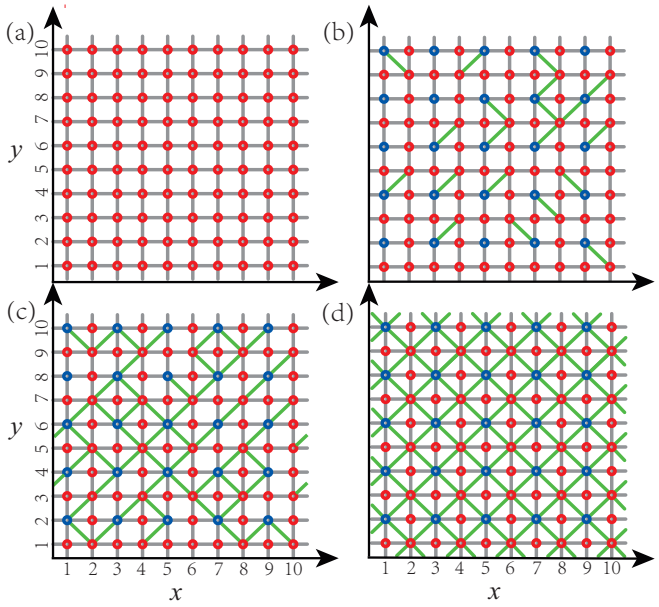

FIG. 1. Schematic illustration of spring networks: (a) square regular network with $N = 10 \times 10$ nodes; [(b),(c)] random networks with average degree, respectively, $\langle k \rangle = 4.4$ and 5.1; (d) regular Union-Jack network with $\langle k \rangle = 6$. The node indices, $1, \ldots, 10$, are ordered along the x and y axes as indicated by the arrows.

Fig. 1(d), known as the Union-Jack lattice [36], with average degree $\langle k \rangle = 6$.

To investigate the influence of network topology on its vibrational properties, we assume that each link connecting two neighboring nodes represents an elastic spring, and the interaction among nodes only occurs through such springs. The dynamics of the resulting elastic network is thus described by the Hamiltonian [34,37]

$$H = \sum_j \frac{p_j^2}{2m} + \frac{1}{2} \sum \left[\sum_{l=1}^{k_j} \frac{1}{2} c_{jl} (u_j - u_l)^2 \right], \qquad (1)$$

where u_j represents the vertical displacement of node j from its equilibrium position, k_j is its degree, and c_{jl} is the spring constant of the link connecting nodes j and l. The motion of any node j, with $j = 1, \ldots N$, obeys the canonical equations [12,38]

$$\dot{u}_j = \frac{\partial H}{\partial p_j}, \quad \dot{p}_j = -\frac{\partial H}{\partial u_j}, \qquad (2)$$

with periodic network boundary conditions. We simulated disordered networks of size $N = 50 \times 50$, with nodes of mass $m = 1$ and spring constants $c_{jl} = 1$ for all links unless stated otherwise. As is well known, the phononic properties of an ideal crystal are characterized by the dispersion relations of its eigenmodes. In sharp contrast, for random spring networks the lack of translational symmetry implies the nonconservation of the phonon modes, i.e., no standard dispersion relations. However, our numerical simulations point to ascending relations between network eigenfrequencies, ω, and mode indices, λ, which can be utilized as pseudodispersion relations. A similar approach was proposed in the past to identify different types of transitions from extended to localized vibrational states in gradient systems [38].

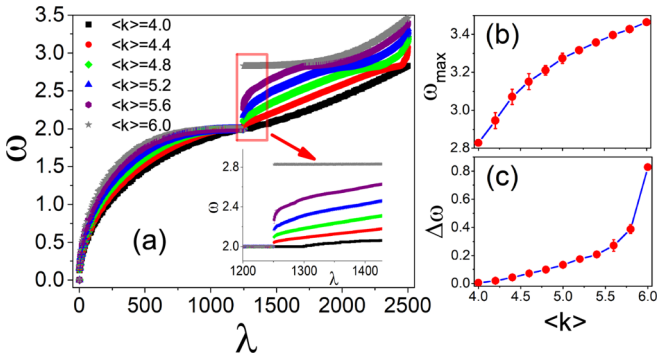

FIG. 2. Examples of random spring network pseudodispersion relations, ω_λ: (a) eigenfrequency, ω, vs eigenmode index, λ, for different $\langle k \rangle$ (see the legend); (b) cutoff frequency, $\omega_{max} = \omega_{\lambda=2500}$, vs $\langle k \rangle$; (c) phonon band gap, $\Delta\omega$, vs $\langle k \rangle$. Simulation data for random spring networks with $n = 50$, $m = 1$, and $c_{lj} = 1$.

III. RESULTS

In this work, we reformulated the node equations of motion, Eq. (2), in terms of the network adjacency matrix, and we developed a pseudodispersion relation formalism, which bridges network topology and the phonon spectrum, and thus provides a theoretical basis to understand the vibrational properties of disordered networks (see Appendix A 1). Figure 2(a) shows the eigenfrequency, ω, versus its eigenmode index, λ, for random spring networks with different average degrees, $\langle k \rangle$. We remark that the curve for $\langle k \rangle = 4.0$ coincides with the usual dispersion relation of the initial regular square lattice. As clearly illustrated in Fig. 2, increasing $\langle k \rangle$ significantly impacts the network pseudodispersion relation, especially at frequencies above $\omega = 2$. Moreover, the eigenfrequency spectrum develops a gap with lower bound $\omega = 2$ and upper bound $\omega < 2.8$, depending on $\langle k \rangle$. In particular, for a given eigenmode index, λ, the larger the average degree $\langle k \rangle$, the larger is the corresponding eigenfrequency, ω_λ. Accordingly, the maximum eigenfrequency (cutoff frequency), $\omega_{max} = \omega_{\lambda=2500}$, increases monotonically with $\langle k \rangle$, as shown in Fig. 2(b).

The region around $\omega = 2$, marked by a red box in Fig. 2(a), has been expanded in the inset. One notices immediately that all curves converge to one value, $\omega = 2$, smoothly for $\lambda \to 1250-$ and with an abrupt drop for $\lambda \to 1250+$, which proves the existence of a band gap between $\lambda = 1250$ and 1251. The width of such a gap, $\Delta\omega = \omega_{\lambda=1251} - \omega_{\lambda=1250}$, is plotted versus $\langle k \rangle$ in Fig. 2(c): as anticipated above, $\Delta\omega$ too is a monotonically increasing function of $\langle k \rangle$. This result suggests a new strategy for tailoring the phonon band gap of disordered networks, that is, by tuning the average degree of the network, a strategy significantly different from traditional approaches, which rely on changing the mechanical parameters of the network (e.g, the node masses, elastic moduli, and the substrate potentials) or applying external fields [39–41]. To better appreciate the impact of the average degree on the network band gap, we developed a mean-field scheme, whereby we

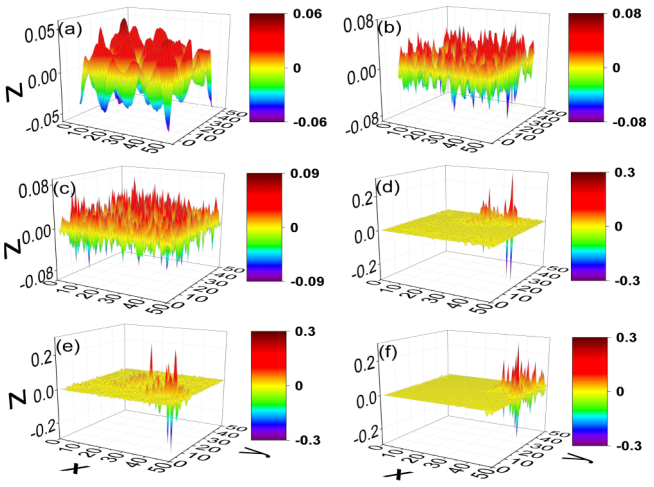

FIG. 3. Eigenmode patterns, e_ω, for (a) $\omega = 0.6245$, (b) $\omega = 1.5037$, (c) $\omega = 1.8512$, (d) $\omega = 2.4452$, (e) $\omega = 2.9397$, and (f) $\omega = 3.1885$. The network lattice rests in the x-y plane, and vertical node displacements, e_j, are oriented along the z axis [see Eq. (3)]. Simulation data for random spring networks with $n = 50$, $m = 1$, $c_{lj} = 1$, $\langle k \rangle = 5.2$, and $r = -0.25$.

started from a Union-Jack lattice [of the kind displayed in Fig. 1(d)] and tuned the coupling strength c' corresponding to the $2N$ diagonal links alone, by gradually increasing it from 0 to 1. By this procedure, we introduce a mean-field definition of $\langle k \rangle = 2c' + 4$, which acts as a control parameter for the transition between the regular network topologies with $\langle k \rangle = 4$ [Fig. 1(a)] and 6 [Fig. 1(d)]. By solving the relevant node equations of motion for $n = 50$, we obtained two dispersion relations, respectively, for the acoustic ($1 \leqslant \lambda \leqslant 1250$) and the optical branch ($1251 \leqslant \lambda \leqslant 2500$). Moreover, increasing $\langle k \rangle$ affects more appreciably the optical branch, thus producing a widening band gap in the range $\omega \in [2, 2\sqrt{2})$ (see Appendix A 2 for details). This analytical description is consistent with the simulation data of Fig. 2.

To analyze in more detail the properties of the pseudodispersion relations of Fig. 2(a), we computed the network density of states for different values of $\langle k \rangle$. For disordered networks with $4 < \langle k \rangle < 6$, the numerical data reveal two sharp peaks located at $\omega = 2$ and 2.8 (see Fig. 6 in Appendix A 3). For $\langle k \rangle \to 6$, the density of states between the two peaks tends to vanish, consistently with the widening of the band gap. Generally, sharp peaks in the density of states, often referred to as Van Hove singularities, point to a transition between different vibrational states. Therefore, we expect that the eigenmodes with frequencies falling in the three domains, $\omega < 2$, $2 < \omega < 2.8$, and $2.8 < \omega$, may have qualitatively distinct features. To clarify this point, we first generated a single disordered network with average degree $\langle k \rangle = 5.2$, and we compared six of its eigenmode patterns, e_ω, in Fig. 3, three with $\omega < 2$, one with $2 < \omega < 2.8$, and two with $\omega > 2.8$. As a first difference, one sees by inspection that the three vibrational modes with $\omega < 2$, Figs. 3(a)–3(c), are extended, whereas the three modes with $\omega > 2$, Figs. 3(d)–3(f), are localized, as most of the lattice nodes sit at rest.

For a more quantitative description of the relation between disorder and mode localization, we then analyzed the eigenmode inverse participation ratio [38]

$$P_\omega^{-1} = \frac{\sum_{j=1}^{N} e_{\omega,j}^4}{\left(\sum_{j=1}^{N} e_{\omega,j}^2\right)^2}, \tag{3}$$

with $e_{\omega,j}$ denoting the node j component of the eigenmode e_ω. This ratio is of the order of $1/N$ for extended modes, and grows to $O(1)$ as the mode excitation is confined to increasingly smaller lattice regions. The ω-dependence of P_ω^{-1} changes with increasing the network average degree in a suggestive manner (see Fig. 7 in Appendix A 4): (i) $\omega < 2$: P_ω^{-1} is always vanishingly small (no localized modes); (ii) $\omega > 2.8$: P_ω^{-1} is large for $\langle k \rangle \gtrsim 4$ but very small for $\langle k \rangle \lesssim 6$ (localized-to-extended mode transition); (iii) $2 < \omega < 2.8$: P_ω^{-1} is large in correspondence with the upper bound of the phonon gap. These findings contradict the common notion that mode localization due to impurities and defects only occurs in crystals, and they prove that it can be produced and governed in complex systems, too.

Another factor affecting the vibrational properties of a disordered network is its degree correlation. A positive (negative) degree correlation refers to the tendency of links to connect nodes with similar (different) degrees (see Appendix A 5). The degree correlation of a network is quantified by its assortativity coefficient [42]

$$r = \frac{\langle k_l k_j \rangle - \langle (k_l + k_j)/2 \rangle^2}{\langle (k_l^2 + k_j^2)/2 \rangle - \langle (k_l + k_j)/2 \rangle^2}, \tag{4}$$

where k_l and k_j are the degrees of two connected nodes l and j, and $\langle \cdots \rangle$ denotes the average over all links. Previous studies revealed that many networked systems, like the Internet or certain proteomic and metabolic networks, may perform distinct functions depending on their assortativity [42–44]. Moreover, both percolation phase transitions and heat conduction can be governed by tuning the degree correlation of the underlying networks [35,42]. These earlier results suggest that the vibrational properties of random spring networks may also depend on their assortativity. To numerically investigate the degree correlation effects, we varied the parameter r of the simulated networks while keeping their average degrees constant (see Appendix A 5 for numerical details).

In Fig. 4(a) we plotted three pseudodispersion relations for a disordered spring network with fixed average degree, $\langle k \rangle = 4.8$, but different values of the parameter r. For $\lambda \leqslant 1250$ all three curves tend to overlap, while for $\lambda > 1250$ they appear to grow steeper with increasing r. To illustrate this point, in the figure insets we expanded the regions around the gap (red box) and the maxima (black box) of the dispersion curves. One notices immediately that the vertical ordering of the curves in the two insets is inverted, consistently with the anticipated r-dependence of their steepness. Accordingly, with increasing r the maximum phonon eigenfrequency, $\omega_{\max}$, becomes larger, but the band gap, $\Delta\omega$, shrinks. The dependence of $\omega_{\max}$ and $\Delta\omega$ on more values of r is displayed in Figs. 4(b) and 4(c). We conclude that $\omega_{\max}$ ($\Delta\omega$) does increase (decrease) monotonically with raising the network degree correlation. This conclusion is confirmed also by numerical data obtained for an additional random spring network with $\langle k \rangle = 5.2$; see Figs. 4(d)–4(f). We remark that the idea of tailoring the phonon band gap of a disordered network of given

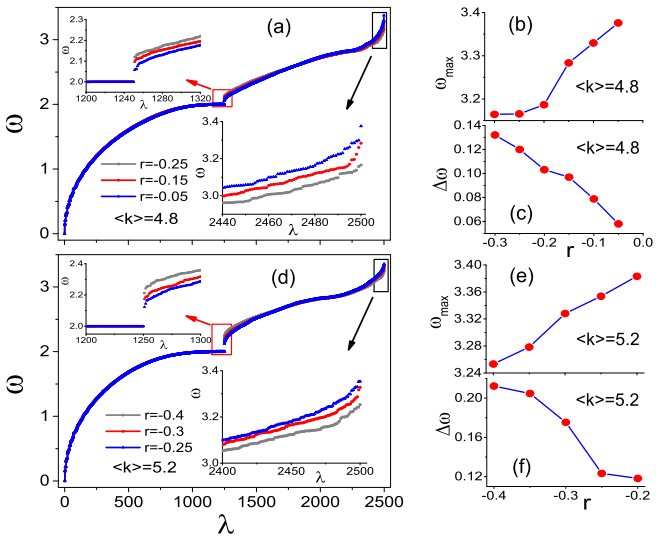

FIG. 4. Dependence of the pseudodispersion relation, ω_λ, of a random spring network on its assortativity coefficient, r: (a) ω vs λ for $\langle k\rangle = 4.8$ and different r (see the legend); [(b),(c)] $\omega_{\max}$ and $\Delta\omega$ vs r for $\langle k\rangle = 4.8$; [(d)–(f)] same as in [(a)–(c)] but for $\langle k\rangle = 5.2$. Simulation data for random spring networks with $n = 50$, $m = 1$, and $c_{lj} = 1$.

average degree by tuning its assortativity coefficient represents a fundamentally new strategy. It is realized by changing the topology of the network rather than its mechanical properties (including the link density) [41]. Furthermore, we find that the assortativity coefficient plays a crucial role in regulating the localization of phonons. Specifically, we observed that the localization intensity of high-frequency phonons decreases as the value of r increases (see Appendix A 8).

Finally, we compared the phononic and wave propagation properties of a random spring network. We injected sine-waves of different frequency, ω, through a source node selected as follows: for waves of frequency corresponding to the eigenfrequency of a localized phonon mode, we made sure to choose a vibrating lattice node [see, e.g., the mode patterns, e_ω, of Figs. 3(d)–3(f)]; for all other frequencies, we picked a network node at random. Based on Eqs. (1) and (2), the source node obeys the equation of motion, $\ddot{u}_j = \sum_{l=1}^{k_j}(u_l - u_j) + u_s - u_j$, with $u_s = A\sin(\omega t)$, and, for simplicity, $A = 1$. We implemented a fourth-order Runge-Kutta algorithm with an integration step of $\Delta t = 0.01$ to simulate the wave propagation through the network. Extensive numerical simulations confirm that the elastic wave propagation properties of the network are consistent with the existence of the predicted extended-to-localized phonon state transitions, and the possibility of controlling the phonon band gap, $\Delta\omega$, and the cutoff frequency, $\omega_{\max}$, by adjusting the topological network parameters, $\langle k\rangle$ and r (see Appendix A 6).

IV. DISCUSSION AND CONCLUSION

In conclusion, we proposed and studied a random spring network model especially designed to investigate the influence of the average degree, $\langle k\rangle$, and the assortativity coefficient, r, on the vibrational properties of a disordered network. By establishing a pseudodispersion relation formalism, we revealed two remarkable properties. First, the pseudodispersion relation markedly depends on the network topological parameters, $\langle k\rangle$ and r. In particular, $\langle k\rangle$ is responsible for the extended-to-localized state transitions of the phonon modes, which is not sensitive to the change of r. Moreover, the cutoff frequency of the phonon spectrum, $\omega_{\max}$, increases monotonically with increasing $\langle k\rangle$ and r. Secondly, the model suggests a novel method to govern the phonon band gap, $\Delta\omega$, in disordered networks, whereby the gap width can be enhanced (or reduced) by increasing $\langle k\rangle$ (or r).

Most notably, these results are independent of the system size, thus confirming that the cutoff frequency and the band gap are primarily determined by the intrinsic characteristics of the networks (see Fig. 14 in Appendix A 7). One might object that $\langle k\rangle$ and r are just two of the many topological characteristics defining the properties of a network. Indeed, the impact of other topological characteristics (such as the clustering coefficient, cycle coefficient, betweenness, and average shortest path) on the vibration properties of the network is still unknown. However, such topological characteristics also reflect on the network adjacency matrix [31,32], which we explicitly linked to the network phononic band gap in this work. The spectrum of the adjacency matrix is known to provide information about various network phenomena, such as disease spreading, stability and convergence of diffusion processes, and the occurrence of extreme events and synchronized states [45]. With this work, we showed how it can also be used to control the vibration properties of random elastic networks for new applications to acoustics and phononics.

Due to its unexpected properties, our random spring network model lends itself to all sorts of applications that require the manipulation of phononic properties and elastic wave propagation in disordered materials. We mention here two examples. The first example involves the tailoring of the phonon bands. Earlier studies have shown that phonon band engineering allows us to fabricate phononic crystals, whose band gap is tunable by means of appropriate substrate potentials and external fields [41]. However, our results indicate that the phonon band gap and cutoff frequency of a random network can also be manipulated by adjusting its connectivity density and correlation. As already remarked above, by tuning the network topology, a fraction of the phonon modes, initially reflected outside the network, are now allowed to propagate [see Figs. 16(a) and 16(b) in Appendix A 9]. This suggests new avenues to customize the phonon properties of a networked material. The second example involves the harvesting of vibrational energy. An acoustic wave can be localized in the cavity of a sonic crystal, where it can be tuned at resonance (point defect mode). Utilizing this phenomenon, one can convert vibrational energy into electric energy by placing a piezoelectric probe into the cavity [46,47]. Similarly, we could remove some nodes from a spring network to generate a defect band in its phonon band gap, so that the impinging acoustic waves get trapped and the piezoelectric probe can harvest electric energy [see Fig. 16(c) in Appendix A 9]. Such a mechanical-to-electric energy conversion method is applicable to the design of intelligent textiles and wearable power sources based on stretchable networked composites [48].

ACKNOWLEDGMENTS

We acknowledge financial support from the National Natural Science Foundation of China under Grants No. 12005166, No. 12035004, and No. 11935010, from the Science and Technology Commission of Shanghai Municipality under Grant No. 20JC1414700, and from the China Postdoctoral Science Foundation under Grants No. 2022M720036 and No. 2023T160110.

APPENDIX

1. Calculation of the pseudodispersion relation of a random spring network

We extend here the dispersion relation formalism for regular elastic lattices to compute the pseudodispersion relations of random spring networks. From the main text, the network Hamiltonian reads [34,37] $H = \sum_j \frac{p_j^2}{2m} + \frac{1}{2}\sum[\sum_{l=1}^{k_j} \frac{1}{2} c_{jl}(u_j - u_l)^2]$ [Eq. (1)], where u_j represents the vertical displacement of node j from its equilibrium position, k_j is the number of the links connecting the node (node degree), and c_{jl} is the spring constant of the link connecting nodes j and l. The motion of any node j, with $j = 1, \ldots, N$, obeys the canonical equations [12,38] $\dot{u}_j = \frac{\partial H}{\partial p_j}$; $\dot{p}_j = -\frac{\partial H}{\partial u_j}$ [Eq. (2)]. Substituting Eq. (1) into Eq. (2) yields

$$\ddot{u}_j = -\frac{\partial H}{\partial u_j} = -\frac{\partial \sum_j V_j(u_j)}{\partial u_j} = \sum_{l=1}^{k_j}(u_l - u_j). \tag{A1}$$

where $V_j(u_j) = \sum_{l=1}^{k_j} \frac{1}{2} c_{jl}(u_j - u_l)^2$ represents the interaction energy of node j with its neighbors. Expanding the displacement u_j in Eq. (A1) in terms of the eigenvector components, $e_{\omega,j}$, of the eigenmodes, e_ω,

$$u_j = \sum_\omega Q_\omega e_{\omega,j}, \tag{A2}$$

with Q_ω the time-dependent expansion coefficient $Q_\omega(t) = \exp(-i\omega t)$, Eq. (A1) can be separated as

$$-\omega^2 e_\omega = T e_\omega. \tag{A3}$$

Due to the assumed periodic network boundary conditions, for $c_{jl} = 1$ the elements of the $N \times N$ coupling matrix T can be rewritten as

$$T_{jl} = A_{jl} - I_{jl}, \tag{A4}$$

where T_{jl} represents the elastic coupling of node j with its neighboring node l, and A_{jl} are the elements of the network adjacency matrix, defined as follows: if node j and l are connected by a spring, then $A_{jl} = 1$, otherwise $A_{jl} = 0$. I is a diagonal matrix with elements $I_{jl} = \delta_{jl} k_j$, where δ denotes the Kronecker delta. The nontrivial N solutions for eigenmodes e_ω and the eigenfrequencies ω in Eq. (A3) were computed by numerically diagonalizing the matrix T.

2. Calculation of the pseudodispersion relation by the mean-field approximation

We introduce here a mean-field technique to tune the average degree, $\langle k \rangle$, of our random network model between 4 and 6, without varying the number of diagonal links [49]. In fact, we analyze a disordered network with reference to the corresponding regular Union-Jack network by treating nodes with degree 4 (red points) and 6 (blue points) separately. In this section, we refer to the color code adopted in Fig. 1(b) of the main text. If only the elastic interactions between neighboring nodes are considered, the equations of motion for the blue and red nodes are, respectively,

$$m\ddot{u}_l = c(4u_j - 4u_l) + c'(4u_j - 4u_l), \tag{A5}$$

$$m\ddot{u}_j = c(4u_l - 4u_j), \tag{A6}$$

where u_l (u_j) are the vertical displacements of the blue (red) points from their equilibrium position, m is the mass of the nodes, and c and c' are the coupling constants corresponding, respectively, to the vertical and horizontal (gray) links and to the diagonal (green) links. Without loss of generality, we set $m = 1$, and $c = 1$ and $c' \in [0, 1]$. We next assume that Eqs. (A5) and (A6) have plane-wave solutions, $u_l = A\exp(i\omega t - d_{ll'}q)$ and $u_j = B\exp(i\omega t - d_{jj'}q)$, where $d_{ll'}$ ($d_{jj'}$) is the Manhattan distance between the lattice points l and l' (j and j') [50], to obtain, by substitution into Eqs. (A5) and (A6),

$$A[\omega^2 - (4 + 4c')] + B(4 + 4c')\cos(q) = 0, \tag{A7}$$

$$4A\cos(q) + B(\omega^2 - 4) = 0. \tag{A8}$$

To ensure that Eqs. (A7) and (A8) have solutions, ω must satisfy the secular equation,

$$\begin{vmatrix} \omega^2 - (4 + 4c') & (4 + 4c')\cos(q) \\ 4\cos(q) & (\omega^2 - 4) \end{vmatrix} \equiv 0, \tag{A9}$$

that is,

$$\omega^4 - (8 + 4c')\omega^2 + (16 + 16c')\sin^2(q) = 0. \tag{A10}$$

The solution of Eq. (A10) yields the two distinct dispersion relations, both periodic functions of q,

$$\omega_+^2 = 4 + 2c' + \sqrt{(4 + 2c')^2 - (16 + 16c')\sin^2(q)}, \tag{A11}$$

$$\omega_-^2 = 4 + 2c' - \sqrt{(4 + 2c')^2 - (16 + 16c')\sin^2(q)}, \tag{A12}$$

plotted in Fig. 5(a). The maximum vibration frequency, $\omega_{\max}$, and the band gap, $\Delta\omega$, depend apparently on c'. Under the mean-field approximation, one easily obtains $\langle k \rangle = 2c' + 4$ and the $\langle k \rangle$-dependence of $\omega_{\max}$ and $\Delta\omega$ plotted in Figs. 5(b) and 5(c). Both $\omega_{\max}$ and $\Delta\omega$ are monotonically increasing functions of $\langle k \rangle$ with upper and lower bounds comparable with those of the simulation curves in Figs. 2(b) and 2(c) of the main text. Discrepancies between numerical simulation and the mean-field approximation emerge when one looks at the convexity of the curves $\omega_{\max}$ and $\Delta\omega$ versus $\langle k \rangle$.

3. Density of states for random spring networks with different average degrees

To examine in detail the $\langle k \rangle$-dependence of the pseudodispersions plotted in Fig. 2(a) of the main text, we computed the

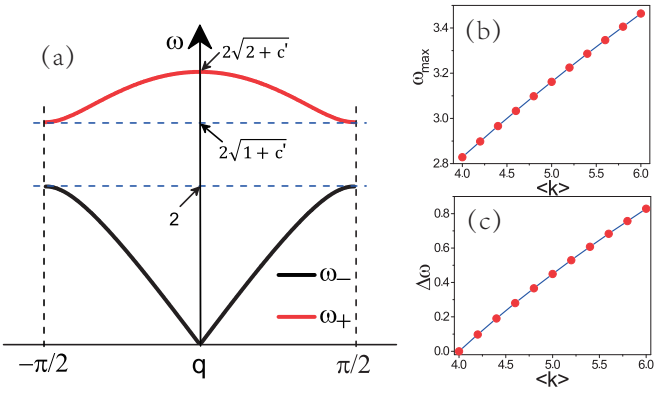

FIG. 5. Phonon band structure of random spring networks in the mean-field approximation: (a) phonon dispersion relation; [(b),(c)] $\omega_{\max}$ and $\Delta\omega$ vs $\langle k\rangle$. Data for networks with $n = 50$, $m = 1$, $c = 1$, and $c' \in [0, 1]$.

density of the phonon states [38],

$$g(\omega) = \lim_{\Delta\omega\to 0} \frac{\Delta n}{\Delta\omega}. \tag{A13}$$

In Fig. 6 we display a few $g(\omega)$ curves for different values of $\langle k\rangle$. [They can be regarded as the inverse of the derivative of the corresponding curves in Fig. 2(a) of the main text.] One notices immediately that $g(\omega)$ exhibits only one peak for $\langle k\rangle = 4$ (regular square lattice) [Fig. 6(a)] and two peaks for $\langle k\rangle > 4$ (random spring networks) [Figs. 6(b)–6(d)]. Note that the two peaks do not move with increasing $\langle k\rangle$; they are always centered, respectively, at $\omega = 2$ and 2.8, in agreement with the analytical predictions of Fig. 5(a).

4. Eigenmode inverse participation ratio for different average degrees

The dependence of the eigenmode inverse participation ratio, P_ω^{-1}, versus the mode eigenfrequency, ω, for random

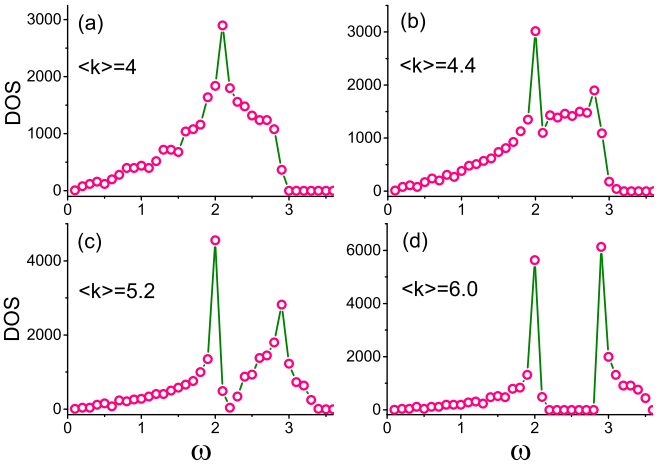

FIG. 6. Phonon density of states (DOS), $g(\omega)$, for different network topologies: (a) regular square lattice with $\langle k\rangle = 4$; [(b),(c)] random spring networks with $\langle k\rangle = 4.4$ and 5.2; (d) regular Union-Jack network with $\langle k\rangle = 6$. Simulation data for spring networks with $n = 50$, $m = 1$, and $c_{lj} = 1$.

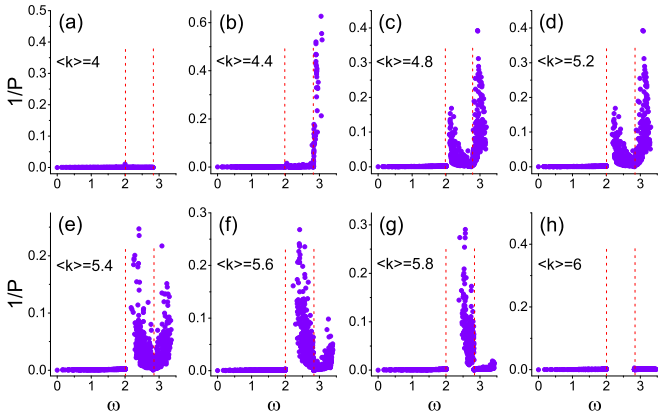

FIG. 7. Eigenmode inverse participation ratio of random spring networks vs the eigenfrequency, ω, for different $\langle k\rangle$: (a) $\langle k\rangle = 4$, (b) $\langle k\rangle = 4.4$, (c) $\langle k\rangle = 4.8$, (d) $\langle k\rangle = 5.2$, (e) $\langle k\rangle = 5.4$, (f) $\langle k\rangle = 5.6$, (g) $\langle k\rangle = 5.8$, and (h) $\langle k\rangle = 6.0$. Simulation data for spring networks with $n = 50$, $m = 1$, and $c_{lj} = 1$.

spring networks of increasing average degree, illustrated in Fig. 7, proves the existence of a transition between extended and localized modes due to disorder. The two $g(\omega)$ singularities at $\omega = 2$ and 2.8, shown in Fig. 6, divide the eigenfrequency domain into three distinct regions, namely $\omega < 2$, $2 < \omega < 2.8$, and $\omega > 2.8$ (marked by red vertical dashed lines in Fig. 7). As $\langle k\rangle$ increases, we notice that P_ω^{-1} for $\omega < 2$ remains close to zero, which means that all vibrational modes are extended, that is, all network nodes oscillate. For $2 < \omega < 2.8$, P_ω^{-1} tends to grow with increasing $\langle k\rangle$, which implies that the vibrational modes in this frequency region change from extended to localized. On the contrary, for $\omega > 2.8$, P_ω^{-1} tends to vanish with increasing $\langle k\rangle$, which signals the opposite transition from localized to extended modes.

It should be emphasized that in the region $2 < \omega < 2.8$, with increasing $\langle k\rangle$, the peak of P_ω^{-1} moves from $\omega = 2$ toward $\omega = 2.8$ (Fig. 7), while the number of eigenmodes diminishes continuously until they totally disappear (Fig. 6). The combination of these two effects results in the onset of the phonon band gap and its continuous widening. This mechanism is consistent with the simulation data discussed in Fig. 2(c) of the main text.

5. Degree correlation of random spring networks

The degree correlation of a network can be quantified by its assortativity coefficient [42] $r = \frac{\langle k_l k_j\rangle - \langle (k_l+k_j)/2\rangle^2}{\langle (k_l^2+k_j^2)/2\rangle - \langle (k_l+k_j)/2\rangle^2}$ [Eq. (4)], where k_l and k_j are the degrees of two connected nodes, l and j, and $\langle\cdots\rangle$ denotes the average over all links. Network configurations with different r are shown in Fig. 8; they have been obtained from the same initial random spring network with $N = 100$ and $\langle k\rangle = 4.8$. In the assortative case, $r = 0.15$, most of the large-degree nodes with $k > 7$ (red circles) are paired with each other. On the contrary, in the disassortative case, $r = -0.2$, most large-degree nodes with $k > 7$ are parted away from each other. It is apparent that the assortative network has the more inhomogeneous structure.

To investigate the effect of the degree correlation on the vibrational properties of a random spring network, we must

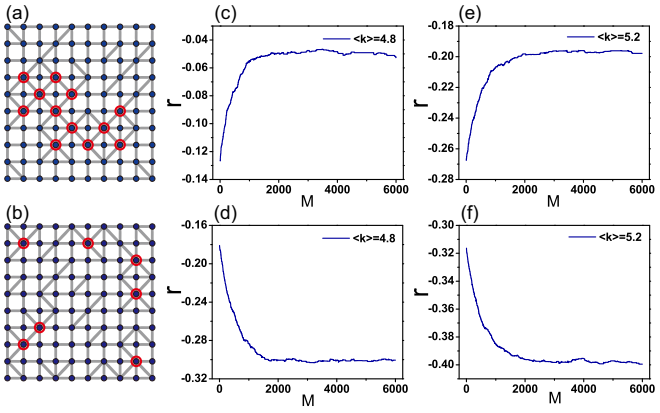

FIG. 8. Regulation of the network assortativity coefficient r. (a) and (b) Snapshots of two random spring networks with $r = 0.15$ and -0.2, respectively. [(c)–(f)] Approximate upper and lower r values corresponding to the average network degrees $\langle k\rangle = 4.8$ [(c),(d)] and $\langle k\rangle = 5.2$ [(e),(f)], respectively, with M denoting the number of iterations.

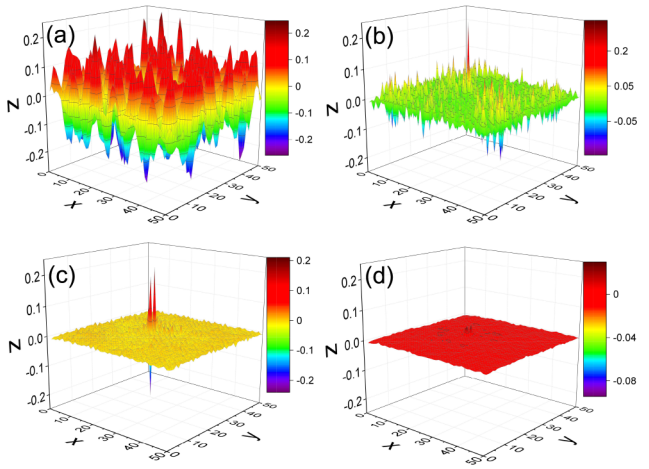

FIG. 9. Propagation transients of sine-waves at time $t = 10^4$ for different frequencies: (a) $\omega = 1.0935$, (b) $\omega = 2.5890$, (c) $\omega = 2.9269$, and (d) $\omega = 3.6$. Simulation data for random spring networks with $n = 50$, $m = 1$, $c_{lj} = 1$, and $\langle k\rangle = 4.4$; node displacements are oriented along the z axis (see color chart on the side).

tune r while keeping the network average degree $\langle k\rangle$ constant [42]. To this purpose, we adopted the following iteration procedure: First, we calculated the assortativity coefficient of a starting network configuration, r_0, through Eq. (4); second, we randomly broke up a diagonal link (i.e., a green link according to the color code of Fig. 1 of the main text), and replaced it by a link connecting another couple of catercorner nodes; finally, we determined whether the assortativity coefficient of the new network configuration, r', came closer to the target value of the coefficient, r, than to its initial value, r_0. If it did, we then utilized an annealing algorithm [51,52] with probability threshold set at $p = 0.01$. If a randomly generated number was greater than p, we retained the above operation; otherwise, we discarded it. This approach significantly increases the algorithm's likelihood of escaping local optimal values, and it enhances the chances of discovering the global optimal value. We repeated the above procedure until $|r' - r| < 0.01$. Using this method, we obtained that the approximate upper and lower assortativity of networks with average degrees is $\langle k\rangle = 4.8$ and 5.2, displayed in Figs. 8(c)–8(f).

6. Elastic wave propagation

In this section, we compare the simulation results of elastic wave propagation in random spring networks and the relevant phonon band characterization based on numerical (see Figs. 2 and 4 of the main text) and analytical predictions (pseudodispersion relations in the mean-field approximation; see Appendix A 2).

(i) Extended to localized mode transitions. Figure 9 shows the propagation transients of sine-waves of different frequencies at $t = 10^4$ for a network with $\langle k\rangle = 4.4$. From Fig. 2 of the main text and Fig. 7, we know that $\omega = 1.0935$ and 2.5890 fall in the range of the extended modes, $\omega = 2.9269$ is in the range of the localized modes, while $\omega = 3.6$ is larger than the cutoff frequency, $\omega_{\max} = 3.0712$. On the other hand, all network nodes are excited in Figs. 9(a), 9(b) only a few in Fig. 9(c), and none in Fig. 9(d). The results of our numerical simulation for wave propagation in a random spring network are thus consistent with the analytical result reported in Fig. 2(b) of the main text.

(ii) Phonon band gap, $\Delta\omega$, versus the average degree, $\langle k\rangle$. Figure 10 shows the propagation transients of a sine-wave of frequency $\omega = 2.0943$ for two networks, respectively, with $\langle k\rangle = 4.0$ and 5.2. From Fig. 2(c) of the main text and Fig. 7, we know that $\omega = 2.0943$ falls in the range of the extended modes for $\langle k\rangle = 4.0$, but in band gap for $\langle k\rangle = 5.2$. One verifies that all network nodes are excited in panel (a), but none in panel (b). This confirms that the phonon band gap, $\Delta\omega$, in disordered networks can be widened by increasing the average degree, $\langle k\rangle$.

(iii) Phonon band gap, $\Delta\omega$, versus the assortativity coefficient, r. Figure 11 shows the propagation transients of sine-waves in networks with different assortativity coefficients: (a),(b) $\omega = 2.0862$ and $\langle k\rangle = 4.8$; (c),(d) $\omega = 2.1398$ and $\langle k\rangle = 5.2$. According to the theoretical results in Fig. 4(c) of the main text, $\omega = 2.0862$ in Figs. 11(a) and 11(b) falls in the band gap for $r = -0.3$, and in the range of the localized modes for $r = -0.05$. On the other hand, all nodes are at rest in Fig. 11(a) and only a few are excited in Fig. 11(b). Moreover, for the network with $\langle k\rangle = 5.2$, Figs. 11(c) and

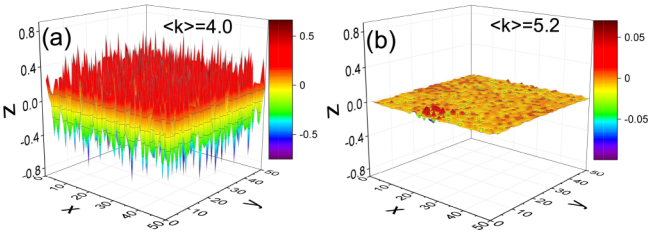

FIG. 10. Propagation transients of a sine-wave of frequency $\omega = 2.0943$ at time $t = 10^4$ in random spring networks with (a) $\langle k\rangle = 4.0$ and (b) $\langle k\rangle = 5.2$. Simulation data for random spring networks with $n = 50$, $m = 1$, and $c_{lj} = 1$; node displacements are oriented along the z axis (see color chart on the side).

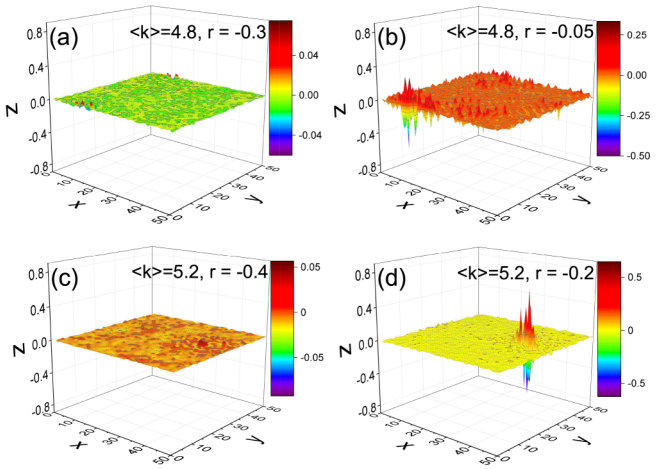

FIG. 11. [(a),(b)] Propagation transients of a sine-wave of frequency $\omega = 2.0862$ at $t = 10^4$ in a random network with $\langle k \rangle = 4.8$ and (a) $r = -0.3$, (b) $r = -0.05$. [(c),(d)] Same as in [(a),(b)] but for $\omega = 2.1398$, $\langle k \rangle = 5.2$, and (c) $r = -0.4$, (d) $r = -0.2$. Simulation data for random spring networks with $n = 50$, $m = 1$, and $c_{lj} = 1$; node displacements are oriented along the z axis (see color chart on the side).

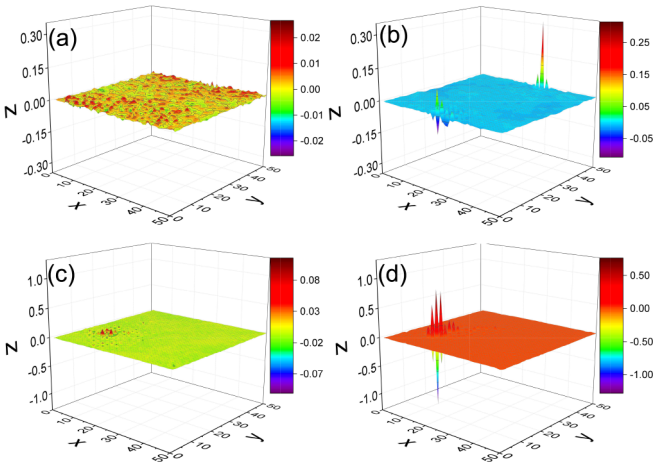

FIG. 13. [(a),(b)] Propagation transients of a sine-wave of frequency $\omega = 3.2662$ at $t = 10^4$ in a random network with $\langle k \rangle = 4.8$ and (a) $r = -0.3$, (b) $r = -0.05$. [(c),(d)] Same as in [(a),(b)] but for $\omega = 3.3171$, $\langle k \rangle = 5.2$, and (c) $r = -0.4$, (d) $r = -0.2$. Simulation data for random spring networks with $n = 50$, $m = 1$, and $c_{lj} = 1$; node displacements are oriented along the z axis (see color chart on the side).

11(d), the frequency $\omega = 2.1398$ is in the band gap for $r = -0.4$, and in the range of the localized modes for $r = -0.2$. Again, no network nodes are excited in Fig. 11(c), and only a few in Fig. 11(d). In conclusion, simulations for networks with different values of $\langle k \rangle$ confirm that the phonon band gap, $\Delta\omega$, of disordered networks shrinks upon increasing the assortativity coefficient, r, for a fixed value of $\langle k \rangle$.

(iv) Cutoff frequency, $\omega_{\max}$, versus the average degree, $\langle k \rangle$. Figure 12 shows the propagation transients of a sine-wave of frequency $\omega = 3.393$ in two networks, respectively, with $\langle k \rangle = 4.2$ and 5.8. According to the theoretical results in Fig. 2(b) of the main text and Fig. 7, $\omega = 3.393$ lies above the cutoff frequency for $\langle k \rangle = 4.2$, but in the localized mode range for $\langle k \rangle = 5.8$. Correspondingly, no network nodes are excited in Fig. 12(a), but most of them are in Fig. 12(b), which confirms that the cutoff frequency, $\omega_{\max}$, is an increasing function of average degree, $\langle k \rangle$.

(v) Cutoff frequency, $\omega_{\max}$, versus the assortativity coefficient, r. Figure 13 shows the propagation transients of sine-waves in networks with different assortativity coefficients: (a),(b) $\omega = 3.2662$ and $\langle k \rangle = 4.8$; (c),(d) $\omega = 3.3171$ and $\langle k \rangle = 5.2$. According to the theoretical results in Fig. 4(b) of the main text and Fig. 7, $\omega = 3.2662$ in Figs. 13(a) and 13(b) lies above the band gap for $r = -0.3$, and in the range of the localized modes for $r = -0.05$. On the other hand, all nodes are at rest in Fig. 13(a) and only a few are excited in Fig. 13(b). Moreover, for the network with $\langle k \rangle = 5.2$, Figs. 13(c) and 13(d), the frequency $\omega = 3.3171$ falls within the band gap for $r = -0.4$, and in the range of the localized modes for $r = -0.2$. Again, no network nodes are excited in Fig. 13(c), and only a few in Fig. 13(d). These results prove that the cutoff frequency, $\omega_{\max}$, of a network of given $\langle k \rangle$ can be raised by increasing the assortativity coefficient, r.

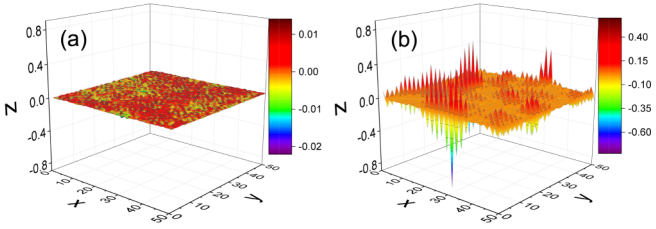

FIG. 12. Propagation transients of a sine-wave of frequency $\omega = 3.393$ at time $t = 10^4$ in random spring networks with (a) $\langle k \rangle = 4.2$ and (b) $\langle k \rangle = 5.8$. Simulation data for random spring networks with $n = 50$, $m = 1$, and $c_{lj} = 1$; node displacements are oriented along the z axis (see color chart on the side).

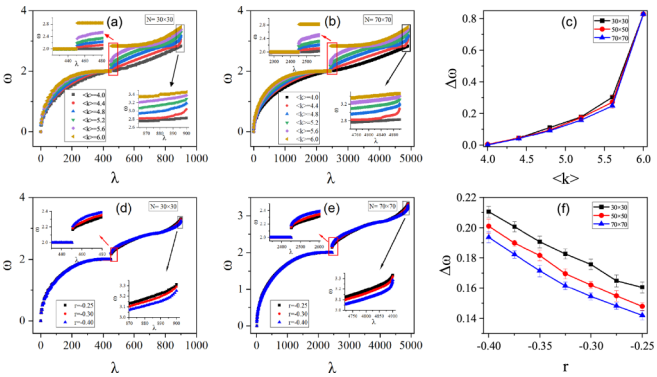

FIG. 14. Dependence of the network spectral properties on its size, N. (a) ω vs λ for $N = 30 \times 30$ and different $\langle k \rangle$. (b) ω vs λ for $N = 70 \times 70$ and different $\langle k \rangle$. (c) $\Delta\omega$ vs $\langle k \rangle$ for different N. Averages were taken over 20 network realizations with fixed $\langle k \rangle$. (d) ω vs λ for $N = 30 \times 30$ and different r. (e) ω vs λ for $N = 70 \times 70$ and different r. (f) $\Delta\omega$ vs r for different N. Averages were taken over 20 network realizations with fixed r.

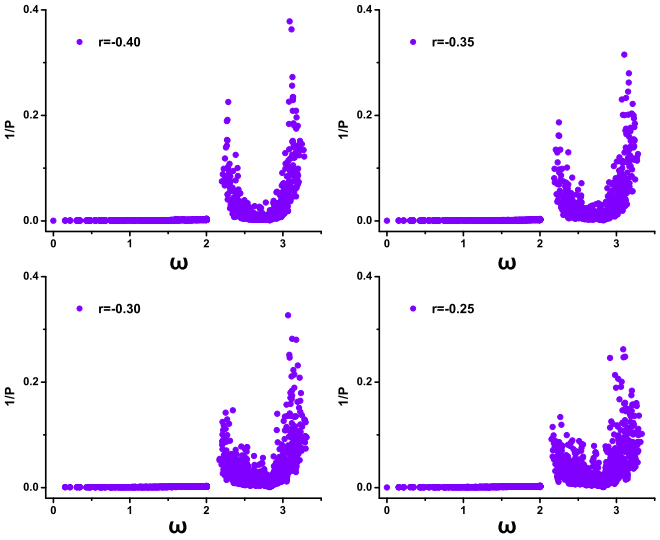

FIG. 15. Eigenmode inverse participation ratio of random spring networks vs the eigenfrequency, ω, for different r: (a) $r = -0.40$, (b) $r = -0.35$, (c) $r = -0.30$, and (d) $r = -0.25$. Simulation data for spring networks with $n = 50$, $m = 1$, and $c_{lj} = 1$.

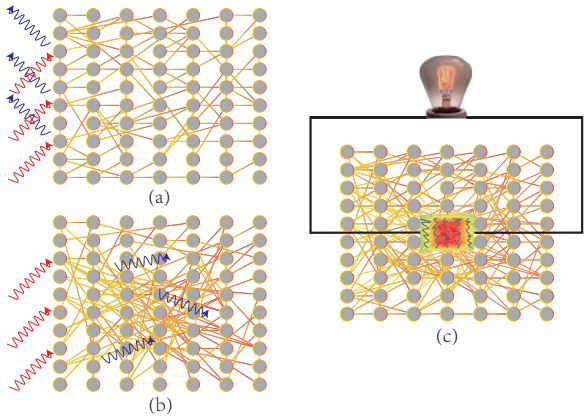

FIG. 16. [(a),(b)] Tailoring of the network phonon bands. The plane waves (red waves) with frequency falling inside the band gap or above the cutoff frequency are reflected at the interface (blue waves) after being injected into the network [panel (a)]. After adjusting the topological structure of the network, its phonon band is modified so as to allow previously reflected waves to propagate through [panel (b)]. (c) Vibrational energy harvesting. A point defect is created inside a random spring network, and a phonon mode localized around it resonates. The defect mode vibration energy can be converted into electrical energy by placing a piezoelectric probe in contact with the defect.

7. Pseudodispersion relation and phononic band gap for different system sizes

Figure 14 shows the pseudodispersion relation, $\omega(\lambda)$, and the phononic band gap, $\Delta\omega$, versus the network average degree, $\langle k\rangle$, and assortativity coefficient, r, for different system sizes. Our results indicate that the width of $\Delta\omega$ slightly decreases with increasing the system size, while other parameters remain unchanged, thus confirming that the band gap is primarily determined by the intrinsic characteristics of the networks.

8. Eigenmode inverse participation ratio of random spring networks for different assortativity coefficient r

The dependence of the eigenmode inverse participation ratio, P_ω^{-1}, versus the mode eigenfrequency, ω, for random spring networks of increasing average degree, is illustrated in Fig. 15. The results demonstrate that as the assortativity coefficient r increases, the localization intensity of high-frequency phonons progressively weakens.

9. Applications

Due to its intriguing properties, our random spring network model has found applications in various fields that involve the manipulation of phononic properties and elastic wave propagation in disordered materials. By leveraging the unique properties of disordered networks, we can advance various technologies and contribute to the development of innovative materials and devices [as shown in Fig. 16].

[1] Y. Jiang, Z. Zhang, Y. X. Wang, D. Li, C. T. Coen, E. Hwaun *et al.*, Science **375**, 1411 (2022).
[2] T. Tsaban, J. K. Varga, O. Avraham, Z. Ben-Aharon, A. Khramushin, and O. Schueler-Furman, Nat. Commun. **13**, 176 (2022).
[3] L. Wang, Z. Wang, C. Wang, and J. Ren, Phys. Rev. Lett. **128**, 067701 (2022).
[4] A. D. Broido and A. Clauset, Nat. Commun. **10**, 1017 (2019).
[5] A. R. Benson, D. F. Gleich, and J. Leskovec, Science **353**, 163 (2016).
[6] M. Szell, R. Lambiotte, and S. Thurner, Proc. Natl. Acad. Sci. USA **107**, 13636 (2010).
[7] X. Xu, A. K. Jha, D. A. Harrington, M. C. Farach-Carson, and X. Jia, Soft Matter **8**, 3280 (2012).
[8] G. Yan, J. Ren, Y. C. Lai, C. H. Lai, and B. Li, Phys. Rev. Lett. **108**, 218703 (2012).
[9] Y. W. Chen, L. F. Zhang, and J. P. Huang, J. Phys. A **40**, 8237 (2007).
[10] N. P. Mitchell, L. M. Nash, D. Hexner, A. M. Turner, and W. Irvine, Nat. Phys. **14**, 380 (2018).
[11] Y. Long, J. Ren, and H. Chen, Phys. Rev. Lett. **124**, 185501 (2020).
[12] M. Kellomaki, J. Astrom, and J. Timonen, Phys. Rev. Lett. **77**, 2730 (1996).
[13] M. Kellomaki, J. Astrom, and J. Timonen, Phys. Rev. E **57**, R1255(R) (1998).
[14] S. Babaee, A. S. Shahsavari, P. Wang, R. C. Picu, and K. Bertoldi, Appl. Phys. Lett. **107**, 211904 (2015).
[15] N. Arora, Y. Xiang, and S. Rudykh, Int. J. Mech. Sci. **200**, 106433 (2021).
[16] J. P. Huang and K. W. Yu, Opt. Lett. **30**, 275 (2005).
[17] R. Anufriev and M. Nomura, Mater. Today. Phys. **15**, 100272 (2020).

[18] B. Graczykowski, N. Vogel, K. Bley, H. J. Butt, and G. Fytas, Nano Lett. **20**, 1883 (2020).
[19] M. A. Lemonde, S. Meesala, A. Sipahigil, M. J. A. Schuetz, M. D. Lukin, M. Loncar, and P. Rabl, Phys. Rev. Lett. **120**, 213603 (2018).
[20] K. Imamura and S. Tamura, Phys. Rev. B **70**, 174308 (2004).
[21] H. Shin, J. A. Cox, R. Jarecki, A. Starbuck, Z. Wang, and P. T. Rakich, Nat. Commun. **6**, 6427 (2015).
[22] A. Agarwala, *Excursions in Ill-Condensed Quantum Matter* (Springer Nature, Switzerland, 2019).
[23] G. Wang, J. P. Huang, and K. W. Yu, Opt. Lett. **35**, 1908 (2010).
[24] M. Petružálek, J. Vilhelm, V. Rudajev, T. Lokajíček, and T. Svitek, Int. J. Rock Mech. Min. **60**, 208 (2013).
[25] A. P. Sarvazyan, M. W. Urban, and J. F. Greenleaf, Ultrasound Med. Biol. **39**, 1133 (2013).
[26] A. B. Khanikaev, R. Fleury, S. H. Mousavi, and A. Alu, Nat. Commun. **6**, 8260 (2015).
[27] C. Heussinger and E. Frey, Phys. Rev. Lett. **97**, 105501 (2006).
[28] Q. Lei and D. Sornette, Europhys. Lett. **136**, 39001 (2021).
[29] D. A. Head, A. J. Levine, and F. C. MacKintosh, Phys. Rev. Lett. **91**, 108102 (2003).
[30] M. Newman, *Networks* (Oxford University Press, New Delhi, 2018).
[31] M. Kivel, A. Arenas, M. Barthelemy, J. P. Gleeson, Y. Moreno, and M. A. Porter, J. Complex Netw. **2**, 203 (2014).
[32] R. Albert and A. L. Barabási, Rev. Mod. Phys. **74**, 47 (2002).
[33] H. Xu, S. Zhang, S. M. Anlage, L. Hu, and G. Grüner, Phys. Rev. B **77**, 075418 (2008).
[34] K. Xiong, C. Zeng, Z. Liu, and B. Li, Phys. Rev. E **98**, 022115 (2018).
[35] K. Xiong, C. Zeng, and Z. Liu, Nonlin. Dyn. **94**, 3067 (2018).
[36] Q. N. Chen, M. P. Qin, J. Chen, Z. C. Wei, H. H. Zhao, B. Normand, and T. Xiang, Phys. Rev. Lett. **107**, 165701 (2011).
[37] Z. Liu and B. Li, Phys. Rev. E **76**, 051118 (2007).
[38] J. J. Xiao, K. Yakubo, and K. W. Yu, Phys. Rev. B **73**, 054201 (2006).
[39] E. G. Charalampidis, J. Lee, P. G. Kevrekidis, and C. Chong, Phys. Rev. E **98**, 032903 (2018).
[40] P. Karki and J. Paulose, Phys. Rev. Appl. **15**, 034083 (2021).
[41] J. Baumgartl, M. Zvyagolskaya, and C. Bechinger, Phys. Rev. Lett. **99**, 205503 (2007).
[42] J. D. Noh, Phys. Rev. E **76**, 026116 (2007).
[43] S. N. Soffer and A. Vazquez, Phys. Rev. E **71**, 057101 (2005).
[44] J. Xiang, K. Hu, Y. Zhang, T. Hu, and J. M. Li, Europhys. Lett. **111**, 48003 (2015).
[45] C. Sarkar and S. Jalan, Chaos **28**, 102101 (2018).
[46] L. Y. Wu, L. W. Chen, and C. M. Liu, Appl. Phys. Lett. **95**, 013506 (2009).
[47] H. Lv, X. Tian, M. Y. Wang, and D. Li, Appl. Phys. Lett. **102**, 034103 (2013).
[48] F. Jiang, X. Zhou, J. Lv, J. Chen *et al.*, Adv. Mater. **34**, 2200042 (2022).
[49] R. Pastor-Satorras and A. Vespignani, Phys. Rev. E **63**, 066117 (2001).
[50] C. L. N. Oliveira, P. A. Morais, A. A. Moreira, and J. S. Andrade, Jr., Phys. Rev. Lett. **112**, 148701 (2014).
[51] S. Kirkpatrick, C. D. Gelatt, and M. P. Vecchi, Science **220**, 671 (1983).
[52] M. Schrauth, J. A. J. Richter, and J. S. E. Portela, Phys. Rev. E **97**, 022144 (2018).